Bollettino di Geofisica Teorica ed Applicata Vol. 60, n. 3, pp. 403-418; September 2019
DOI 10.4430/bgta0258

# Anelasticity of porous rocks containing microcracks: a reformulation of the BISQ model

C. Wu[1], J. Ba[1], L. Zhang[1] and J.M. Carcione[1,2]

[1] *School of Earth Sciences and Engineering, Hohai University, Nanjing, P.R. China*
[2] *Istituto Nazionale di Oceanografia e di Geofisica Sperimentale - OGS, Sgonico (TS), Italy*

(Received: 1 August 2018; accepted: 13 November 2018)

***ABSTRACT*** The BISQ model unified the Biot theory and the squirt-flow mechanism. The squirt flow is induced by the compression of the pore volume due to the wave excitation and pressure gradients between stiff pores and microcracks. On the basis of this model, we consider the fluid in microcracks to oscillate perpendicular to the wave direction, which is independent of the global (Biot) wave oscillation. The BISQ theory is, then, reformulated in terms of the law of conservation of fluid mass and the crack aspect ratio and density, hereafter called Re-BISQ model. The BISQ model is a particular case of the Re-BISQ model if the microcrack porosity to total porosity ratio is set to one. We analyse the effects of rock properties, such as the permeability and the characteristic squirt length. Comparisons with ultrasonic experimental data indicate that the Re-BISQ model provides a better description of the wave properties than the original BISQ model.

**Key words:** anelastic wave propagation, BISQ model, Biot theory, squirt-flow, wave dissipation, poroelasticity.

## 1. Introduction

Theoretical studies of wave propagation in reservoirs are developed from a single-porosity medium to more complex pore systems. The study of waves in a single-porosity medium started in the 1950s, when Gassmann (1951) investigated the effects of pore fluids on the elastic properties without considering the relative motion between the fluid and the skeleton. Biot (1956a, 1956b, 1962) established the basic theory of dynamic poroelasticity in a saturated porous solid. The theory laid the foundation for studying waves in a fluid/solid two-phase system and predicted the existence of slow P-wave, which was confirmed in experiment by Plona (1980). However, it is widely accepted that the Biot theory cannot sufficiently explain the strong attenuation phenomena observed in real rocks (Mavko and Nur, 1975; White, 1975; Dvorkin and Nur, 1993; Carcione, 2014; Ba *et al*., 2018; Wang *et al*., 2018). The main reason is that the model assumes that the pores are unique and homogeneous (a single-porosity medium) and fluids only flow in the direction of wave propagation. These basic assumptions are inconsistent with the internal complexities of actual rocks.

To improve the description of wave propagation, White (1975) first presented the concept of mesoscopic non-uniformity and patchy-saturation (spherical gas patches) (White model) to

 

explain the strong wave attenuation, but the low frequency limit is inconsistent with Gassmann (1951) theoretical model. Dutta and Ode (1979a, 1979b), Dutta and Seriff (1979c), and Carcione (2014) solved this inconsistency. Based on White model, Berryman and Wang (1995) obtained the constitutive relations of a double-porosity medium. Subsequently, Berryman and Wang (2000) developed the dynamic equations of elastic wave propagation in a double-porosity dual-permeability medium, and studied the wave dispersion and attenuation. Pride and Berryman (2003a, 2003b) derived the equations of wave propagation in a double-porosity medium based on volume average. Ba *et al*. (2011, 2014, 2016) derived the Biot-Rayleigh equations for wave propagation in double-porosity rocks based on the Hamiltonian principle. Then, Ba *et al*. (2015, 2017) presented a double double-porosity model based on the Biot-Rayleigh equations and considered the heterogeneous characteristics of the pore-fluid patchy-saturation and double-porosity structure of actual reservoirs. The model can be used to describe the wave propagation characteristics in partially-saturated complex reservoirs. Guo *et al*. (2018) applied the model in analysing wave velocity dispersion and attenuation in fluid saturated tight sandstones. Sun *et al*. (2016) and Zhang *et al*. (2017) proposed the triple-porosity model for wave propagation in reservoir rocks.

On the other hand, the influence of the microscopic local fluid flow on wave propagation has also been considered and investigated. Mavko and Nur (1975) considered a squirt-flow mechanism based on pore microscopic geometry, which successfully explained the high wave dispersion and attenuation. However, the theory highly relies on the pore geometry. Therefore, this model is difficult to apply and separates the Biot and squirt flows, which is inconsistent with a real physical process. Dvorkin and Nur (1993) presented a BISQ (Biot/squirt) model based on the assumption that the pores are saturated with a single fluid. The BISQ model combines the Biot and squirt flows into same mechanical model, so that the high velocity dispersion and attenuation can be explained. Subsequently, Dvorkin *et al*. (1994) further extended the BISQ model to partially saturated conditions by modifying the characteristic squirt length. Diallo and Appel (2000) and Diallo *et al*. (2003) tried to reformulate the characteristic squirt length to improve the BISQ model. However, the predicted P-wave velocity dispersion and attenuation move to the high frequencies when the rock permeability decreases, and this is at odds with the prediction of the original BISQ model. Cheng *et al*. (2002) introduced a viscoelastic mechanism into the BISQ model, and Nie *et al*. (2008) added viscoelastic into BISQ model and applied it to muddy sandstones. The viscoelastic BISQ model can be used to explain the high dispersion and attenuation in the low frequencies band, but it is not a predictive model, only a phenomenological approach. Gurevich *et al*. (2010) and Carcione and Gurevich (2011) presented an alternative squirt-flow model, in which the parameters can be entirely estimated from the microstructural properties of the rock.

Tang (2011) stated that the BISQ model does not involve two important parameters: the crack density and the crack aspect ratio, and he derived the wave equations by incorporating these parameters. In this work, we generalise the BISQ model to contain explicitly the influence of penny-shape cracks on wave propagation. The BISQ model is reformulated from the perspective of fluid mass conservation. The reformulated model presents the actual wave propagation characteristics in reservoir rocks.

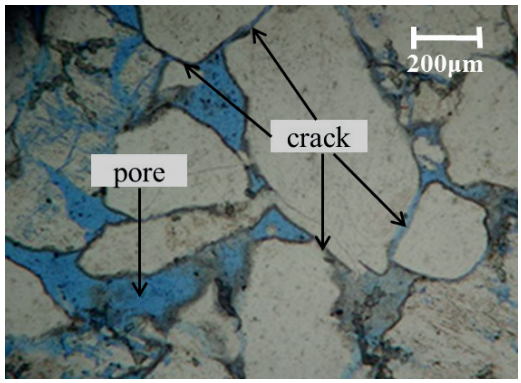


Fig. 1 - Microcracks and inter-granular pores in a thin section analysis of a tight sandstone.

## 2. Reformulated BISQ equations by incorporating microcrack porosity

As shown in Fig. 1 for a typical tight sandstone, the rock can be assumed as made of two components, the main inter-granular (stiff) pores and the grain contacts or microcracks, whose aspect ratio is very low and their compressibility is much higher than that of the pores.

Dvorkin and Nur (1993) combined the Biot and squirt flows in the same model, considering a cylindrical geometry, as shown in Fig. 2a. The fluid pressure due to local flow outside the sample is constant, and we set it zero for convenience. The constant-pressure boundary is equivalent to the "no-flow boundary" when the microcrack scale is much less than wavelength. Since fluid pressure is constant at the boundary (not affected by the wave oscillations), it will not drive local fluid flow. Dvorkin and Nur (1993) assumed the situation of rocks with very small volumes of gas trapped at the tips of the cracks, which is in line with the natural reservoirs. If a porous rock at 100% full saturation is considered, pore fluid is pushed from thin cracks into the surrounding large pores with pressure in these pores changing in time. Pressure variation in cracks is much larger than that in large pores. Therefore, attenuation and dispersion can still be well estimated by the model.

The radius of this cylinder ($R$) is the characteristic squirt-flow length, which is of the order of the average pore size. Dvorkin and Nur (1993) assumed that this microscale parameter is a fundamental rock property and does not relate to frequency and fluid properties. It indicates the relaxed distance of the fluid when the squirt flow occurs inside the rock. When a seismic wave propagate in the rock, pore fluid flows from the thin cracks into the surrounding inter-granular pores or adjacent cracks with different orientations (Mavko and Nur, 1975). Dvorkin and Nur (1993) did not distinguish the microcracks from the main pores when analysing the squirt flow, which occurs to the fluid in the microcracks, as shown in Fig. 2b, where $\phi$ is the total porosity and $\phi_c$ is the crack porosity.

The Biot (1956a, 1956b) dynamic equations for wave propagation in a two-phase solid/fluid composite are:

$$(1-\phi)\rho_s \frac{\partial^2 u}{\partial t^2} + \phi\rho_f \frac{\partial^2 w}{\partial t^2} = M\frac{\partial^2 u}{\partial x^2} - \alpha\frac{\partial P}{\partial x}, \tag{1a}$$

$$\phi\rho_f \frac{\partial^2 w}{\partial t^2} - \rho_a\left(\frac{\partial^2 u}{\partial t^2} - \frac{\partial^2 w}{\partial t^2}\right) - \frac{\eta\phi^2}{\kappa}\left(\frac{\partial u}{\partial t} - \frac{\partial w}{\partial t}\right) = -\phi\frac{\partial P}{\partial x}, \tag{1b}$$

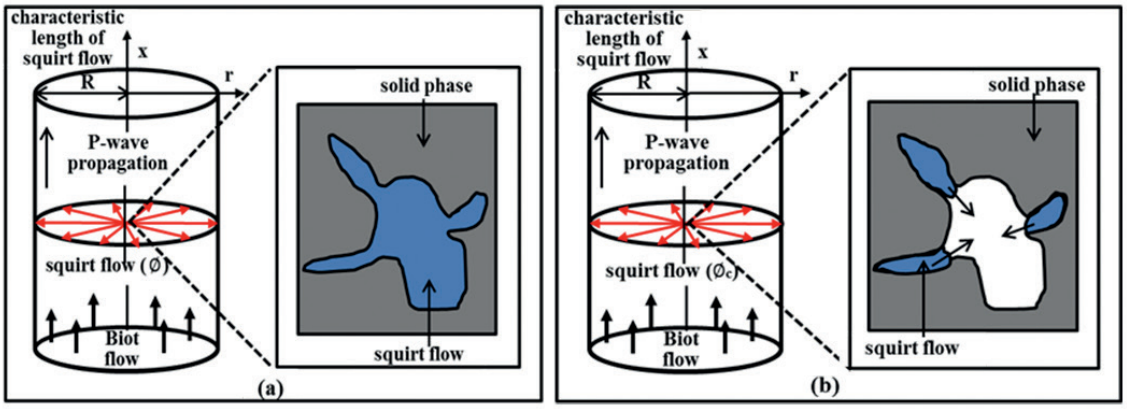


Fig. 2 - Scheme of BISQ model (a) and Re-BISQ (b) where different partition of pore fluid is considered in the squirt-flow process.

where $t$ is time, $\kappa$ and $\eta$ are permeability and viscosity, respectively; $u$ and $w$ are the skeleton and fluid displacement vectors, respectively; $\rho_s$, $\rho_f$, and $\rho_a$ are the solid, fluid and coupling densities, respectively; $M$ is the Biot modulus; $P$ is fluid pressure; $\alpha$ is the poroelasticity coefficient of effective stress, where $\alpha = 1\text{-}K_{dry} / K_0$. $K_{dry}$ is the bulk modulus of the drained skeleton, and $K_0$ is the bulk modulus of the solid.

When a rock is squeezed, the pore fluid squirts from the thin cracks into the surrounding stiff pores or the adjacent cracks with different orientations. According to the conservation of fluid mass, the following equation holds:

$$\frac{\partial\left(\rho_f\phi\right)}{\partial t}+\frac{\partial\left[\rho_f\left(\phi w_t-\phi u_t\right)\right]}{\partial x}+\frac{\partial\left(\rho_f D\phi v_t\right)}{\partial r}+\frac{\rho_f D\phi v_t}{r}=0. \tag{2}$$

where $D$ is the volume ratio of crack porosity to total porosity as $D = \phi_c/\phi$, and $v$ is the fluid displacement in the $r$-direction. If the wavelength is much larger than the crack length, in a local area around every single crack it can be considered as the iso-stress state. Only the principle stress in the perpendicular direction is considered. For each crack, it can be simplified as the model displayed in Fig. 2b. The crack porosity is $\phi_c = 4\pi\zeta\varepsilon/3$ where $\zeta$ is the crack aspect ratio and $\varepsilon$ is the crack density (David and Zimmerman, 2012).

The porosity differential is related to the differentials of the skeleton deformation and fluid pressure as follows (Biot, 1941; Rice and Cleary, 1976):

$$\frac{\partial\phi}{\partial t}=\alpha\frac{\partial^2 u}{\partial x\partial t}+\frac{1}{Q}\frac{\partial P}{\partial t}. \tag{3}$$

$$\mathrm{d}\rho_f=\mathrm{d}P/c_0^2, \tag{4}$$

Substituting Eqs. 3 and 4 into Eq. 2, we can relate pressure to displacements as:

$$P_t=-F\left(w_{xt}+\frac{\gamma}{\phi}u_{xt}+Dv_{rt}+\frac{D}{r}v_t\right), \tag{5}$$

where:

$$\frac{1}{Q} = \frac{1}{K_0}\left(1 - \phi - \frac{K_{dry}}{K_0}\right),$$

$$F = \left(\frac{1}{\rho_f c_0^2} + \frac{1}{\phi Q}\right)^{-1},$$

and $c_0$ is the fluid acoustic velocity.

### *2.1. Dynamical equations*

We have to obtain a dynamical equation in the *r*-direction which complements Eqs. 1a and 1b in the *x*-direction. The equation can be derived from the Lagrange equations with a dissipation function as (Biot, 1956a, 1956b):

$$\left(D\phi\rho_f + \rho_a\right)v_{tt} + \frac{\eta\left(D\phi\right)^2}{\kappa}v_t = -D\phi P_r. \tag{6}$$

The expressions of the *r*-direction fluid displacement and the microcrack fluid pressure are:

$$v\left(x,r,t\right) = v_0\left(r\right)e^{i(1x-\omega t)}, \tag{7a}$$

$$P\left(x,r,t\right) = P_0\left(r\right)e^{i(1x-\omega t)}. \tag{7b}$$

where 1 is the wavenumber, $\omega$ is the angular frequency, and $i$ is the imaginary number.

Substituting Eqs. 7a and 7b into Eq. 6, the fluid pressure gradient equation in the *r*-direction is:

$$\frac{\partial P_0}{\partial r} = v_0\rho_f\omega^2\left(\frac{D\phi + \rho_a/\rho_f}{D\phi} + iD\frac{\omega_c}{\omega}\right). \tag{8}$$

where $\omega_c = \eta\phi/\kappa\rho_f$.

### *2.2. Pore-fluid pressure*

We consider that both the displacements of the solid and the fluid in the *x*-direction are affected by the values of pressure and fluid displacement averaged at the *r*-direction. The solid and fluid displacements in the *x*-direction are:

$$u\left(x,t\right) = C_1e^{i(1x-\omega t)}, \tag{9a}$$

$$w\left(x,t\right) = C_2e^{i(1x-\omega t)}, \tag{9b}$$

where $C_1$ and $C_2$ are constants (see the Appendix). By substituting Eqs. 7 to 9 into Eq. 5, a differential equation describing the fluid pressure dependence on the *r*-coordinate is:

$$\frac{\partial^2 P_0}{\partial r^2} + \frac{1}{r}\frac{\partial P_0}{\partial r} + P_0\frac{\rho_f\omega^2}{DF}\left(\frac{D\phi + \rho_a/\rho_f}{D\phi} + iD\frac{\omega_c}{\omega}\right) = -i1\left(\gamma C_1 + \phi C_2\right)\frac{\rho_f\omega^2}{D\phi}\left(\frac{D\phi + \rho_a/\rho_f}{D\phi} + iD\frac{\omega_c}{\omega}\right). \tag{10}$$

We use a constant pressure boundary condition at $r = R$ to solve this equation, where $R$ is the radius of the representative cylindrical volume and is equal to the characteristic squirt-flow length (Fig. 2b). The result is:

$$P_0(r) = -i\omega\left(\gamma C_1 + \phi C_2\right)\frac{F}{\phi}\left(1 - \frac{J_0\left(\lambda_{Re} r\right)}{J_0\left(\lambda_{Re} R\right)}\right),$$

where $J_0$ is the Bessel function of order zero and:

$$\lambda_{Re}^{\ 2} = \frac{\rho_f \omega^2}{F}\left(\frac{D\phi + \rho_a / \rho_f}{D\phi} + iD\frac{\omega_c}{\omega}\right).$$

The average fluid pressure can be obtained from the previous Eqs. 7 and 9 as:

$$P_{av} = \frac{1}{\pi R^2}\int_0^R 2\pi r P(x,r,t)dr$$

$$= -F\left[1 - \frac{2J_1\left(\lambda_{Re} R\right)}{\lambda_{Re} R J_0\left(\lambda_{Re} R\right)}\right]\left(w_x + \frac{\gamma}{\phi}u_x\right), \tag{11}$$

The partial derivative of Eq. 11 gives:

$$\frac{\partial P_{av}}{\partial t} = -F\left[1 - \frac{2J_1\left(\lambda_{Re} R\right)}{\lambda_{Re} R J_0\left(\lambda_{Re} R\right)}\right]\left(w_{xt} + \frac{\gamma}{\phi}u_{xt}\right), \tag{12}$$

where $J_1$ is the Bessel function of order one. By assuming the following relationship:

$$F_{Re} = F\left[1 - \frac{2J_1\left(\lambda_{Re} R\right)}{\lambda_{Re} R J_0\left(\lambda_{Re} R\right)}\right]. \tag{13}$$

### *2.3. P-wave velocity and attenuation*

It is assumed that the average local flow pressure can be used as the actual fluid pressure in the dynamical Eqs. 1b (Dvorkin and Nur, 1993). According to the relationship between wavenumber and P-wave velocity and attenuation (Toksöz and Johnston, 1981), the expressions of P-wave velocity ($V_p$) and attenuation factor ($a$) are obtained. The derivation is given in the Appendix.

$$V_{p1,2} = \frac{1}{\mathrm{Re}\left(X_{1,2}\right)}, \qquad a_{1,2} = \omega\,\mathrm{Im}\left(X_{1,2}\right), \tag{14}$$

where:

$$X_{1,2} = \sqrt{Y_{1,2}},$$

$$Y_{1,2} = -\frac{B}{2A} \pm \sqrt{\left(\frac{B}{2A}\right)^2 - \frac{C}{A}},$$

$$A = \frac{\phi F M}{\rho_2^2},$$

$$B=\frac{F\left(2\alpha-\phi-\phi\frac{\rho_1}{\rho_2}\right)-\left(M+F\frac{\alpha^2}{\phi}\right)\left(1+\frac{\rho_a}{\rho_2}+i\frac{\omega_c}{\omega}\right)}{\rho_2},$$

$$C=\frac{\rho_1}{\rho_2}+\left(1+\frac{\rho_1}{\rho_2}\right)\left(\frac{\rho_a}{\rho_2}+i\frac{\omega_c}{\omega}\right),$$

$$\rho_1=(1-\phi)\rho_s,\ \rho_2=\phi\rho_f.$$

The values of $X_{1,2}, Y_{1,2}, A, B$, and $C$ are calculated for $F_{Re}=F$. The P-wave velocity and attenuation factor of the Re-BISQ model are obtained.

The BISQ model does not consider the two porosities (microcracks and inter-granular) separately (the microcracks are treated as inter-granular pores). In the above Eqs. 2 and 6, we obtain the BISQ model by setting $D = 1$. Then the two models are equivalent.

## 3. Numerical examples

The results of the Re-BISQ, BISQ and Biot models are compared on the basis of the same rock properties (Berryman, 1980). The porosity is $\phi$=15%, the bulk modulus of the drained skeleton is $K_{dry}=16\times10^9$ Pa, the Poisson's ratio is $\upsilon$=0.15, the density and bulk modulus of solid phase are $\rho_s = 2650$ kg/m$^3$ and $K_0 = 38\times10^9$ Pa, respectively, the permeability is $\kappa=1\times10^{-15}$ m$^2$, the pore-fluid density is $\rho_f = 1000$ kg/m$^3$, its viscosity is $\eta = 0.001$ Pad·s, the fluid bulk modulus is $K_f=2.25\times10^9$ Pa, the coupling density is $\rho_a = 420$ kg/m$^3$, the characteristic length of the squirt flow is $R$=1 mm and the microcrack aspect ratio and density are $\zeta$=0.02 and $\varepsilon$=0.15, respectively.

### *3.1. First model results*

The results are presented in Fig. 3. At ultrasonic frequencies, the P-wave velocity (Fig. 3a) and attenuation (Fig. 3b) calculated with the Re-BISQ model are greater than those calculated by the BISQ model. The peak frequency of the squirt-flow mechanism is less than the characteristic frequency of the Biot flow, which is shown in Fig. 3b. When the frequency $\omega\rightarrow\infty$, the fast P-wave velocity and attenuation values of the Re-BISQ model are the same as those calculated by the Biot model. The values of the fast P-wave velocity of the Re-BISQ model are slightly different from those of the BISQ model, as shown in Fig. 3a. In Fig. 3b, the attenuation obtained with the Re-BISQ model in the frequency range of $10^3$-$10^5$ Hz is higher than that calculated with the BISQ model, whereas the attenuation of the Re-BISQ model is smaller than that calculated with the BISQ model at frequencies >$10^5$ Hz. The value of fast P-wave attenuation of the Re-BISQ model approaches that calculated by the Biot model as frequency increases. The dominant role is the macroscopic Biot flow mechanism at high frequencies, and the microscopic local fluid flow in the frequency range of $10^3$-$10^5$ Hz.

Figs. 3c and 3d show that the values of the slow P-wave velocity and attenuation calculated with the Re-BISQ model are higher than those of the BISQ and Biot models in the low frequency range. The difference is small. The values of the Re-BISQ and BISQ models are similar. The results of the three models are the same at the high-frequency limit.

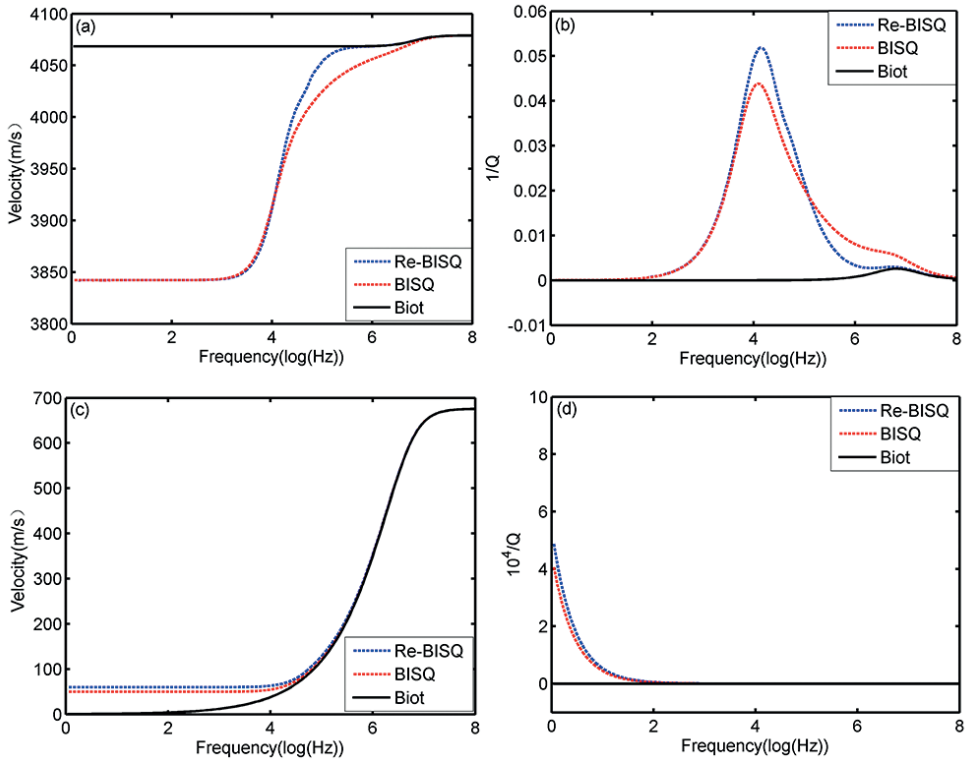


Fig. 3 - Velocity and dissipation factor of the Biot, BISQ, and Re-BISQ models: a) fast P-wave velocity; b) fast P-wave inverse quality factor; c) slow P-wave velocity; d) slow P-wave inverse quality factor.

### *3.2. Effect of crack aspect ratio*

In order to investigate the effect of crack aspect ratio on wave propagation, the same set of rock properties are used except for a varying crack aspect ratio of 0.02, 0.04, and 0.06. The results are shown in Fig. 4.

It is shown in Fig. 4a that the fast P-wave velocity decreases slightly as the aspect ratio increases in the frequency range around the inflection point. At the low-frequency limit, the values for different aspect ratios are the same. In Fig. 4b, the attenuation decreases with increasing aspect

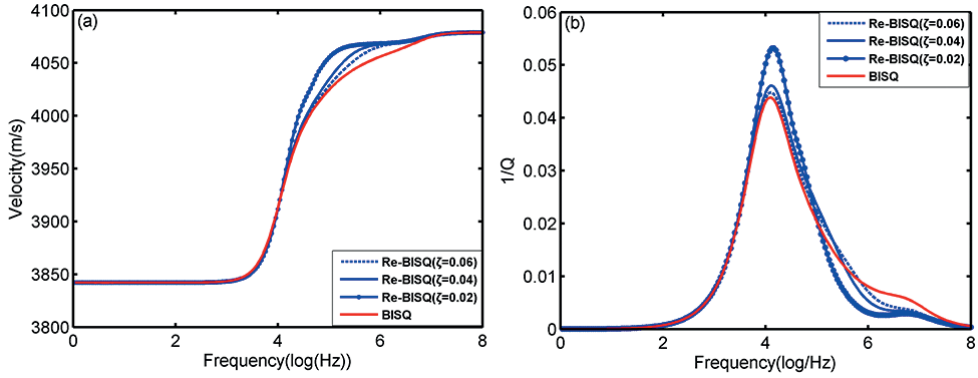


Fig. 4 - Effect of crack aspect ratio on: a) fast P-wave velocity and b) fast P-wave inverse quality factor.

ratio, which gradually approaches the attenuation results of the BISQ model. When the aspect ratio increases, the attenuation of the squirt flow due to microcracks decreases.

### *3.3. Effect of viscosity*

The same rock parameters except for a varying viscosity of 0.1 Pa·s, 0.01 Pa·s, and 0.001 Pa·s are used to analyse the effect of viscosity on wave propagation. The results are given in Fig. 5.

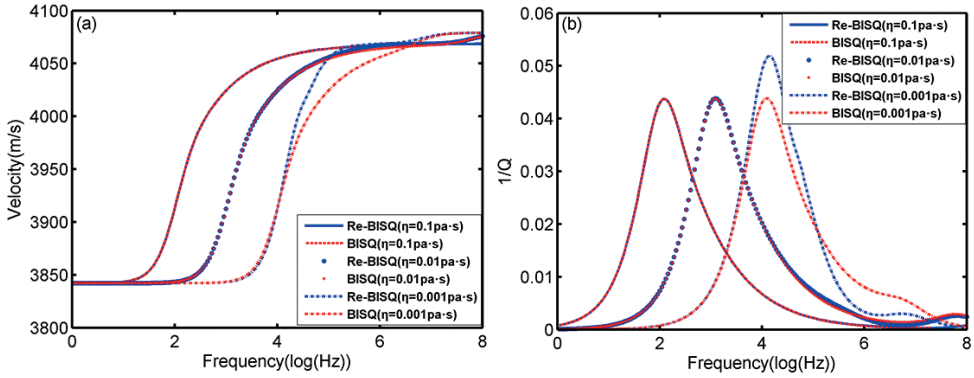


Fig. 5 - Effect of fluid viscosity on: a) fast P-wave velocity and b) fast P-wave inverse quality factor.

The fast P-wave velocity dispersion and attenuation shift to low frequencies as viscosity increases. The effect is consistent with the trend predicted by the BISQ model. It is generally believed that the squirt-flow mechanism mainly affects wave propagation at the sonic or higher frequencies with a low fluid viscosity (Pride and Berryman, 2003a; Pride *et al*., 2004; Deng *et al*., 2012). The physical explanation is that rocks are easier to relax with when the fluid viscosity is low.

### *3.4. Effect of the characteristic squirt-flow length*

Here we consider the characteristic squirt-flow lengths of 1, 2, and 3 mm. The results are shown in Fig. 6. The attenuation peaks and velocity inflection point of the Re-BISQ model shift towards the low frequencies as the characteristic squirt-flow length increases. This effect is consistent with the BISQ model.

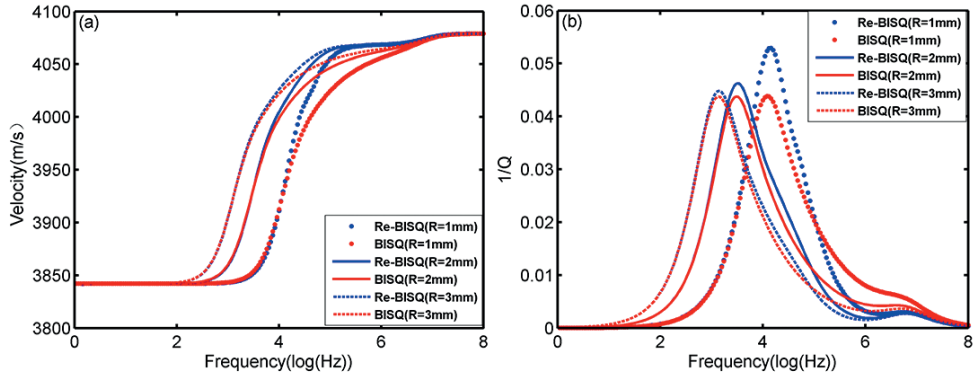


Fig. 6 - Effect of characteristic squirt-flow length on: a) fast P-wave velocity and b) fast P-wave inverse quality factor.

### *3.5. Effect of permeability on wave propagation*

The permeability values are 0.1, 0.5, and 1.0 mD. The attenuation peaks and velocity inflection of the Re-BISQ model shift towards the high frequencies as the permeability increases, which is consistent with the trend predicted by the BISQ model (Fig. 7).

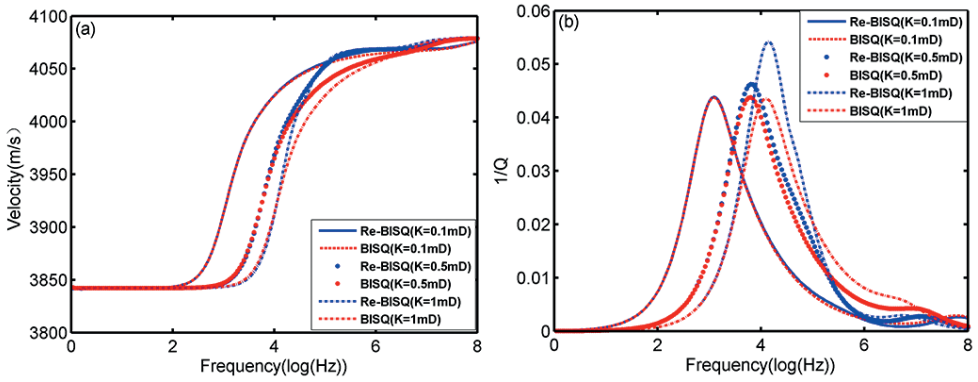


Fig. 7 - Effect of permeability on: a) fast P-wave velocity and b) fast P-wave inverse quality factor.

The wave attenuation inverse quality factor as a function of permeability is given in Fig. 8, where the rock permeability is in the range <300 mD and the wave frequency is 10 kHz.

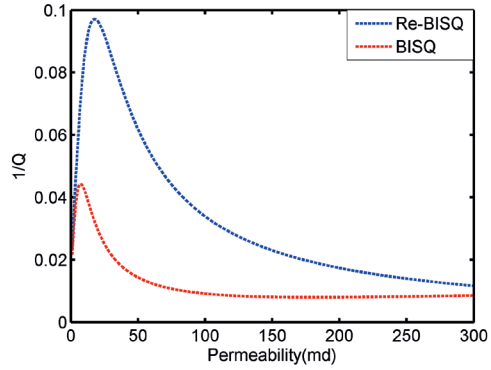


Fig. 8 - Wave dissipation (1/Q) as a function of permeability.

As the permeability increases, the attenuation sharply rises to a maximum value and then decreases (Fig. 8). The attenuation reaches the peak at the permeability of approximately 10 mD. The characteristics are consistent with the squirt-flow attenuation/frequency function (Akbar *et al.*, 1993). At low permeabilities, the pore fluid is unrelaxed and attenuation is small (corresponding to the high-frequency limit), while at high permeabilities, the pore fluid is relaxed, which again results in a small attenuation (corresponding to the low-frequency limit). The Re-BISQ model generally produces high attenuation than the BISQ model. As the permeability increases, the attenuation predicted by the two models tends to be the close. As the permeability increases, the fluid in microcracks tends to be relaxed under wave excitations. Therefore, the attenuation values predicted by the two models decrease and approach the Biot dissipation.

## 4. Comparisons between model results and experimental data

In order to verify the Re-BISQ model, we select experimental data for sandstones and tight sandstones. The predictions of the Re-BISQ and BISQ models are then compared.

### *4.1. Sandstones with a nearly-constant porosity*

Ten saturated sandstones with a nearly-constant porosity are selected from Klimentos and McCann (1990), where ultrasonic (1 MHz) velocity and attenuation were measured at a confining pressure of 40 MPa. The porosity of each rock is $\phi$=15±2%, the fluid bulk modulus is $K_f$=2.25×10$^9$ Pa, and the pore fluid density is $\rho_f$=1000 kg/m$^3$. It is shown in Dvorkin *et al*. (1994) that when the permeability is larger than 100 mD, the measured and the BISQ-predicted attenuation/permeability relationships are very close. It can be observed from the results in Fig. 8 that when the permeability is high, the attenuations predicted by the two models are close to each other.

Here, the permeability of each selected rock sample is less than 100 mD. The rock properties are shown in Table 1.

Table 1 - Properties of the 10 sandstone samples from Klimentos and McCann (1990).

| Sample no. | Porosity (%) | Clay (%) | *Vp* (m/s) | Permeability (mD) | Measured attenuation coefficient (dB/cm) |
|---|---|---|---|---|---|
| 1 | 15.46 | 15.00 | 4152 | 0.05 | 3.15 |
| 2 | 13.47 | 14.00 | 4498 | 0.06 | 4.92 |
| 3 | 16.65 | 12.00 | 4010 | 0.37 | 2.36 |
| 4 | 16.71 | 8.00 | 4381 | 0.44 | 1.57 |
| 5 | 17.13 | 12.00 | 3933 | 2.21 | 2.68 |
| 6 | 13.11 | 7.00 | 4666 | 3.67 | 2.10 |
| 7 | 15.13 | 4.00 | 4794 | 11.06 | 1.65 |
| 8 | 16.50 | 15.00 | 4149 | 41.54 | 3.63 |
| 9 | 16.11 | 15.00 | 4152 | 50.71 | 3.30 |
| 10 | 15.41 | 5.00 | 4246 | 52.42 | 3.38 |

The comparison between the attenuation predicted by the two models (Re-BISQ and BISQ) and the experimental data are shown in Fig. 9. The attenuation predicted by the Re-BISQ model agrees better with the experimental data (Fig. 9), particularly for permeabilities higher than 10 mD.

### *4.2. Tight sandstones in a given porosity range*

The tight sandstones samples were collected from the Sulige Gas Field in the Ordos Basin, NW China. The data of the tight sandstones were reported by Wang (2016). We selected ten water-saturated tight sandstone samples at a confining pressure of 29 MPa. Experimental set-up, conditions, and procedures are given in Wu *et al*. (2000) and Wang *et al*. (2006). The experimental temperature is 105 °C, and the frequency is 1 MHz. The fluid bulk modulus is $K_f$=2.25×10$^9$ Pa and the pore fluid density is $\rho_f$=1000 kg/m$^3$. The data are given in Table 2.

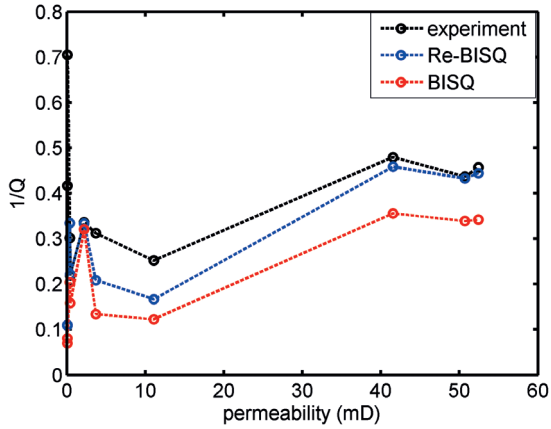


Fig. 9 - Comparison between the two models and the experimental data for sandstones.

Table 2 - Properties of ten tight sandstones (from Wang, 2016).

| Sample no. | Porosity (%) | Permeability (mD) | Matrix bulk modulus (GPa) | Inverse quality factor 1/Q |
|---|---|---|---|---|
| 1 | 3.81 | 0.0300 | 39 | 0.044366 |
| 2 | 4.08 | 0.0424 | 39 | 0.071839 |
| 3 | 4.20 | 0.0443 | 39 | 0.045372 |
| 4 | 4.98 | 0.0591 | 39 | 0.075529 |
| 5 | 5.20 | 0.0641 | 39 | 0.054113 |
| 6 | 5.53 | 0.0724 | 39 | 0.052056 |
| 7 | 5.62 | 0.0748 | 39 | 0.059453 |
| 8 | 6.44 | 0.1013 | 39 | 0.058893 |
| 9 | 6.81 | 0.1161 | 39 | 0.061350 |
| 10 | 7.19 | 0.1336 | 39 | 0.081699 |

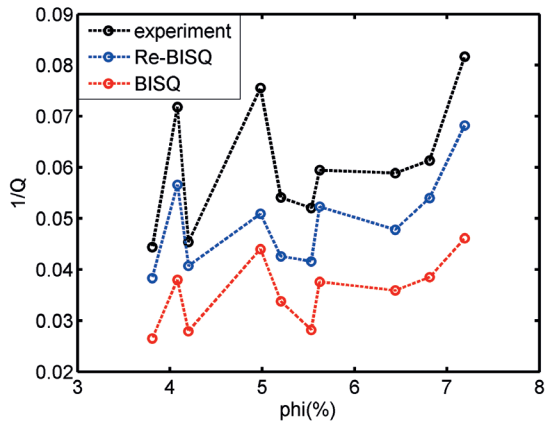


Fig. 10 - Comparison between the two models and the experimental data for tight sandstones.

The comparison between the attenuation predicted by the two models and the experimental data are given in Fig. 10. The attenuation predicted by the Re-BISQ model is closer to the experimental data, although both sets of prediction results seem to underestimate the observed P-wave attenuation.

## 5. Conclusions

Previous studies have shown that microcracks have an important influence on wave propagation. In this work, we consider the distinction between (penny-shaped) microcracks and inter-granular pores in deriving the governing equations of squirt flow affecting wave propagation. The approach is based on the conservation of fluid mass. The basic assumptions of the BISQ model are adopted, and we reformulate the wave equations by incorporating the effect of crack porosity and aspect ratio. The new model (Re-BISQ) can better explain the effects of rock heterogeneity on wave dissipation and velocity dispersion. Comparisons between models and experimental data for P-wave attenuation show that the Re-BISQ model is capable of providing a better description of the observed phenomena for sandstones. This reformulated theory provides a mathematic approach to compute and predict wave responses in heterogeneous reservoirs, and therefore it can be useful for reservoir fluid seismic characterisation.

**Acknowledgements.** We thank Geza Seriani, Jack Dvorkin and the anonymous reviewer for helpful suggestions. This work is supported by the Specially-Appointed Professor Program of Jiangsu Province, China, the Cultivation Program of "111" Plan of China (BC2018019) and the Fundamental Research Funds for the Central Universities, China.

REFERENCES

Akbar N., Dvorkin J. and Nur A.; 1993: *Relating P-wave attenuation to permeability*. Geophys., **58**, 20-29.

Ba J., Carcione J.M. and Nie J.X.; 2011: *Biot-Rayleigh theory of wave propagation in double-porosity media*. J. Geophys. Res., Solid Earth, **116**, B06202.

Ba J., Zhang L., Sun W.T. and Hao Z.B.; 2014: *Velocity field of wave-induced local fluid flow in double-porosity media*. Sci. Chin. Phys. Mech. Astron., **57**, 1020-1030, doi:10.1007/s11433-014-5442-0.

Ba J., Carcione J.M. and Sun W.T.; 2015: *Seismic attenuation due to heterogeneities of rock fabric and fluid distribution*. Geophys. J. Int., **202**, 1843-1847.

Ba J., Zhao J., Carcione J.M. and Huang X.; 2016: *Compressional wave dispersion due to rock matrix stiffening by clay squirt flow*. Geophys. Res. Lett., **43**, 6186-6195.

Ba J., Xu W., Fu L., Carcione J.M. and Zhang L.; 2017: *Rock anelasticity due to patchy saturation and fabric heterogeneity: a double double-porosity model of wave propagation*. J. Geophys. Res., Solid Earth, **122**, 1949-1976, doi:10.1002/2016JB013882.

Ba J., Zhang L., Wang D., Yuan Z., Cheng W., Ma R. and Wu C.F.; 2018: *Experimental analysis on P-wave attenuation in carbonate rocks and reservoir identification*. J. Seismic Explor., **27**, 371-402.

Berryman J.G.; 1980: *Confirmation of Biot's theory*. Appl. Phys. Lett., **37**, 382-384.

Berryman J.G. and Wang H.F.; 1995: *The elastic coefficients of double-porosity models for fluid transport in jointed rock*. J. Geophys. Res., Solid Earth, **100**, 24611-24627.

Berryman J.G. and Wang H.F.; 2000: *Elastic wave propagation and attenuation in a double-porosity dual-permeability medium*. Int. J. Rock Mech. Min. Sci., **37**, 63-78.

Biot M.A.; 1941: *General theory of three-dimensional consolidation*. J. Appl. Phys., **12**, 155-164.

Biot M.A.; 1956a: *Theory of propagation of elastic waves in a fluid-saturated porous solid. I: Low frequency range*. J. Acoust. Soc. Am., **28**, 168-178.

Biot M.A.; 1956b: *Theory of propagation of elastic waves in a fluid-saturated porous solid. II: Higher frequency range*. J. Acoust. Soc. Am., **28**, 179-191.

Biot M.A.; 1962: *Mechanics of deformation and acoustic propagation in porous media*. J. Appl. Phys., **33**, 1482-1498.

Carcione J.M.; 2014: *Wave fields in Real Media. Wave propagation in anisotropic, anelastic, porous and electromagnetic media, 3rd ed*. Elsevier Sci., Amsterdam, The Netherlands, 690 pp.

Carcione J.M. and Gurevich B.; 2011: *Differential form and numerical implementation of Biot's poroelasticity equations with squirt dissipation*. Geophys., **76**, N55-N64.

Cheng Y.F., Yang D.H. and Yang H.Z.; 2002: *Biot/squirt model in viscoelastic porous media*. Chin. Phys. Lett., **19**, 445-448.

David E.C. and Zimmerman R.W.; 2012: *Pore structure model for elastic wave velocities in fluid-saturated sandstones*. J. Geophys. Res., Solid Earth, **117**, B07210.

Deng J.X, Wang S.X and Du W.; 2012: *A study of the influence of mesoscopic pore fluid flow on the propagation properties of compressional wave-a case of periodic layered porous media*. Chin. J. Geophys., **55**, 2716-2727, in Chinese.

Diallo M.S. and Appel E.; 2000: *Acoustic wave propagation in saturated porous media: reformulation of the Biot/squirt flow theory*. J. Appl. Geophys., **44**, 313-325.

Diallo M.S., Prasad M. and Appel E.; 2003: *Comparison between experimental results and theoretical predictions of P-wave velocity and attenuation at ultrasonic frequency*. Wave Motion, **37**, 1-16.

Dutta N.C. and Ode H.; 1979a: *Attenuation and dispersion of compressional waves in fluid-filled porous rocks with partial gas saturation (White model) - Part I: Biot theory*. Geophys., **44** ,1777-1788.

Dutta N.C. and Ode H.; 1979b: *Attenuation and dispersion of compressional waves in fluid-filled porous rocks with partial gas saturation (White model) - Part II: Results*. Geophys., **44**, 1789-1805.

Dutta N.C. and Seriff A.J.; 1979c: *On White's model of attenuation in rocks with partial saturation*. Geophys., **44**, 1806-1812.

Dvorkin J. and Nur A.; 1993: *Dynamic poroelasticity: a unified model with the Squirt and the Biot mechanisms*. Geophys., **58**, 524-533.

Dvorkin J., Hoeksema R.N. and Nur A.; 1994: *The squirt-flow mechanism: macroscopic description*. Geophys., **59**, 428-438.

Gassmann F.; 1951: *Uber die Elastizitat poroser Medien*. Vierteljiahrsschrift der Naturforschenden Geselschaft in Zurich, **96**, 1-23, in German.

Guo M.Q., Ba J., Ma R.P., Chen T.S., Zhang L., Pang M.Q. and Xie J.Y.; 2018: *P-wave velocity dispersion and attenuation in fluid-saturated tight sandstones: characteristics analysis based on a double double-porosity structure model description*. Chin. J. Geophys., **61**, 1053-1068, (in Chinese).

Gurevich B., Makarynska D., Pervukhina M. and De Paula O.; 2010: *A simple model for squirt-flow dispersion and attenuation in fluid-saturated granular rocks*. Geophys., **75**, N109–N120.

Klimentos T. and McCann C.; 1990: *Relationships among compressional wave attenuation, clay content, and permeability in sandstones*. Geophys., **55**, 998-1014.

Mavko G.M. and Nur A.; 1975: *Melt squirt in the asthenosphere*. J. Geophys. Res., **80**, 1444-1448.

Nie J.X., Yang D.H. and Yang H.Z.; 2008: *A generalized viscoelastic Biot/squirt model for clay-bearing sandstones in a wide range of permeabilities*. Appl. Geophys., **5**, 249-260.

Plona T.J.; 1980: *Observation of a second bulk compressional wave in a porous medium at ultrasonic frequencies*. Appl. Phys. Lett., **36**, 259-261.

Pride S.R. and Berryman J.G.; 2003a: *Linear dynamics of double-porosity dual-permeability materials. I. Governing equations and acoustic attenuation*. Phys. Rev. E: Stat. Nonlinear Soft Matter Phys., **68**, 036603.

Pride S.R. and Berryman J.G.; 2003b: *Linear dynamics of double-porosity dual-permeability materials. II. Fluid transport equations*. Phys. Rev. E: Stat. Nonlinear Soft Matter Phys., **68**, 036604.

Pride S.R., Berryman J.G. and Harris J.M.; 2004: *Seismic attenuation due to wave-induced flow*. J. Geophys. Res., Solid Earth, **109**, B01201.

Rice J.R. and Cleary M.P.; 1976: *Some basic stress diffusion solutions for fluid-saturated elastic porous media with compressible constituents*. Rev. Geophys., **14**, 227-241.

Sun W., Ba J. and Carcione J.M.; 2016: *Theory of wave propagation in partially saturated double-porosity rocks: a triple-layer patchy model*. Geophys. J. Int., **205**, 22-37.

Tang X.M.; 2011: *A unified theory for elastic wave propagation through porous media containing cracks-An extension of Biot's poroelastic wave theory*. China Earth Sci., **54**, 1441-1452, (in Chinese).

Toksöz M.N. and Johnston D.H.; 1981: *Seismic wave attenuation*. Soc. Expl. Geophys., Geophys. reprint series 2, Tulsa, OK, USA, 459 pp.

Wang D., Ding P. and Ba J.; 2018: *Analysis of dynamic fracture compliance based on poroelastic theory. Part II: results of numerical and experimental Tests*. Pure Appl. Geophys., **175**, 2987-3001.

Wang D.X.; 2016: *Study on the rock physics model of gas reservoirs in tight sandstone*. Chin. J. Geophys., **59**, 4603-4622, in Chinese.

Wang D.X., Xin K.F., Li Y.M., Gao J.H. and Wu X.Y.; 2006: *An experimental study of influence of water saturation on velocity and attenuation in sandstone under stratum conditions*. Chin. J. Geophys., **49**, 908-914, in Chinese.

White J.E.; 1975: *Computed seismic speeds and attenuation in rocks with partial gas saturation*. Geophys., **40**, 224-232.

Wu X.Y., Chen Z. and Wei J.N.; 2000: *A technique for measuring ultrasonic velocity and attenuation spectra*. Chin. J. Rock Mech. Eng., **19**, 895-898, (in Chinese).

Zhang L., Ba J., Yin W., Sun W.T. and Tang J.Y.; 2017: *Seismic wave propagation equations of conglomerate reservoirs: a triple-porosity structure model*. Chin. J. Geophys., **60**, 1073-1087, doi:10.6038/cjg20170320, in Chinese.

## Appendix: Derivation of P-wave velocity and attenuation

The amplitude of a plane wave can be expressed as $A(x,t)=A_0 e^{i(1x-\omega t)}$. Attenuation may be introduced by allowing the wavenumber to be complex (Toksöz and Johnston, 1981; Carcione, 2014): 1=Re(1)+i Im(1). The attenuation coefficient ($a$) and P-wave velocity ($V_p$) are:

$$a = \mathrm{Im}(1), V_p = \omega / \mathrm{Re}(1). \tag{A1}$$

The inverse quality factor $Q^{-1}$ is related to the coefficient and P-wave velocity as $Q^{-1} = 2aV_p/\omega$. The expressions of solid displacement, fluid displacement and pressure are:

$$u(x,t) = C_1 e^{i(1x-\omega t)}, \tag{A2a}$$

$$w(x,t) = C_2 e^{i(1x-\omega t)}, \tag{A2b}$$

$$p(x,t) = P_0 e^{i(1x-\omega t)}. \tag{A2c}$$

by substituting Eqs. A2a, A2b, and A2c into Eqs. 1a and 1b, and using $P_t = -F\,(w_{xt}+\gamma u_{xt} / \phi)$ (Dvorkin and Nur, 1993), the following relation is obtained:

$$C_1\left[Y\frac{1}{\rho_2}\left(M+\frac{\alpha\gamma F}{\phi}\right)-\frac{\rho_1}{\rho_2}\right]+C_2\left(Y\frac{\alpha F}{\rho_2}\right)=0, \tag{A3a}$$

$$C_1\left(Y\frac{\gamma F}{\rho_2}+\frac{\rho_a}{\rho_2}+i\frac{\omega_c}{\omega}\right)+C_2\left(Y\frac{\phi F}{\rho_2}-1-\frac{\rho_a}{\rho_2}-i\frac{\omega_c}{\omega}\right)=0, \tag{A3b}$$

where: $Y = (1/\omega)^2$, $\rho_1 = (1-\phi)\,\rho_s$, and $\rho_2 = \phi\rho_f \varrho$.

Eqs. A3a and A3b have nonzero solutions for the constants $C_1$ and $C_2$, only if the determinant is equal to zero, which leads to the following equation for $Y$:

$$AY^2 + BY + C = 0, \tag{A4}$$

This equation has two solutions:

$$Y_{1,2} = -\frac{B}{2A} \pm \sqrt{\left(\frac{B}{2A}\right)^2 - \frac{C}{A}}.$$

Therefore, we obtain two values for the ratio $1/\omega$:

$$X_{1,2} = \left(\frac{1}{\omega}\right)_{1,2} = \sqrt{Y_{1,2}},$$

as well as:

$$1_{1,2} = \omega X_{1,2}.$$

The P-wave velocity and attenuation expressions are then:

$$V_{p_{1,2}} = \frac{1}{\mathrm{Re}\left(X_{1,2}\right)}, \quad a_{1,2} = \omega\,\mathrm{Im}\left(X_{1,2}\right). \tag{A5}$$

*Corresponding author:* Jing Ba
School of Earth Sciences and Engineering, Hohai University
Nanjing 211100, P.R. China
Phone: +86 152 10571198; e-mail: jba@hhu.edu.cn